

# Dalton Transactions

Accepted Manuscript



This is an *Accepted Manuscript*, which has been through the Royal Society of Chemistry peer review process and has been accepted for publication.

*Accepted Manuscripts* are published online shortly after acceptance, before technical editing, formatting and proof reading. Using this free service, authors can make their results available to the community, in citable form, before we publish the edited article. We will replace this *Accepted Manuscript* with the edited and formatted *Advance Article* as soon as it is available.

You can find more information about *Accepted Manuscripts* in the [Information for Authors](#).

Please note that technical editing may introduce minor changes to the text and/or graphics, which may alter content. The journal's standard [Terms & Conditions](#) and the [Ethical guidelines](#) still apply. In no event shall the Royal Society of Chemistry be held responsible for any errors or omissions in this *Accepted Manuscript* or any consequences arising from the use of any information it contains.



Journal Name

ARTICLE

## Iron-based inorganic-organic hybrid and superlattice thin films by ALD/MLD

Received 00th January 20xx,  
Accepted 00th January 20xx

DOI: 10.1039/x0xx00000x

www.rsc.org/

A. Tanskanen and M. Karppinen\*

Here we present novel layer-by-layer deposition processes for the fabrication of inorganic-organic hybrid thin films of the (-Fe-O-C<sub>6</sub>H<sub>4</sub>-O)<sub>n</sub> type and also superlattices where thicker iron oxide layers alternate with monomolecular-thin organic layers. The processes are based on a combination of atomic layer deposition (ALD) and molecular layer deposition (MLD) techniques where cyclopentadienyl iron dicarbonyl dimer (Cp<sub>2</sub>Fe<sub>2</sub>(CO)<sub>4</sub>) is used as the iron source and hydroquinone (HQ) as the organic precursor. For the (-Fe-O-C<sub>6</sub>H<sub>4</sub>-O)<sub>n</sub> hybrid films a growth rate value as high as 3.7 Å/cycle was achieved at 180 °C. Superlattices where thin crystalline iron oxide layers of the magnetite structure alternate with single organic layers consisting of benzene rings were moreover successfully fabricated from the same precursors at 160 °C using water as the source of oxygen in the ALD cycles for the magnetite layers. We foresee that our new ALD/MLD processes offer a valuable novel tool to modify the properties of magnetite thin films and even more widely possess the potential to boost the ALD/MLD research frontier on functional transition metal oxide based thin films.

### Introduction

The trend in the future electronic devices is towards smaller, more efficient and more complex; the other demands concern the price, safety and environmental issues when new materials or processes are searched for the next-generation devices. Among the new enabling materials, various transition metal compounds are attractive as they possess exciting electronic and magnetic properties due to their unpaired d-orbital valence electrons.

Iron is the most abundant metal in the Earth, cheap to produce and relatively harmless to the environment and health. Iron oxides, magnetite (Fe<sub>3</sub>O<sub>4</sub>) and hematite (α-Fe<sub>2</sub>O<sub>3</sub>), are particularly interesting, the former being a high-temperature ferromagnet, the latter showing a combination of a relatively small band-gap (2.1 eV) and related visible light absorption, and also stability under deleterious chemical conditions. The reason why iron oxides have not been applicable in large scale in electronics is the limitations in their electrical properties, such as the short charge carrier lifetime and diffusion length.<sup>1,2</sup> Nevertheless, iron-based materials definitely form one of the bases of non-toxic and affordable materials for our next-generation devices, which gives a good motivation to develop and modify them to better respond to the demands in electronics.

Thin films often have higher sensitivity, faster response and lower power consumption when compared with

corresponding bulk materials. Iron oxides have been deposited as thin films with *e.g.* chemical vapour deposition,<sup>3</sup> sol-gel,<sup>4,5</sup> electrodeposition,<sup>6</sup> Langmuir-Blodgett,<sup>7</sup> pulsed laser deposition<sup>8</sup> and atomic layer deposition<sup>6,9,10</sup> techniques. These thin films have potential for *e.g.* gas sensitive materials,<sup>7,9</sup> thermoelectric materials,<sup>8</sup> and photoanode materials in solar cells.<sup>2,6</sup> An obvious drawback of inorganic thin films in general is that they are brittle and cannot necessarily be employed in flexible applications.

Atomic layer deposition (ALD) has gained its reputation as a technique to deposit conformal and pinhole-free thin films even on high-aspect-ratio structures.<sup>11,12</sup> This currently strongly emerging success story in semiconductor industry is mostly due to the possibility to control the film deposition in an atomic-layer level. Then, the newer variant of the technique, *i.e.* molecular layer deposition (MLD), can be used to deposit organic thin films with an accuracy of a molecular layer.<sup>13,14</sup> What is most attractive, by combining these two layer-by-layer gas-phase deposition schemes it is possible to create completely new inorganic-organic hybrid materials with exciting properties.<sup>15–18</sup> When the process is optimized the amount of precursors needed is minimized and since no solvents or other additive chemicals are needed the amount of produced waste is essentially lower than in case of liquid-phase techniques, which makes the ALD/MLD technique besides its other advantages a truly green fabrication technology for the hybrid materials.

<sup>a</sup> Department of Chemistry, Aalto University, P.O. Box 16100, FI-00076 Aalto, Finland, e-mail. Maarit.karppinen@aalto.fi

The combined ALD/MLD technique has already been utilized to deposit aluminium,<sup>19</sup> zinc,<sup>20–22</sup> titanium<sup>23,24</sup> and zirconium<sup>25</sup> based hybrid inorganic-organic thin films with various organic components from simple aliphatic chains to longer conjugated chains and aromatic rings. By adding organic molecules between inorganic atomic layers we can not only enhance the flexibility of the material, but also *e.g.* modify its optical and electrical properties, and enhance its water or gas barrier properties as has been demonstrated by fabricating nanolaminate, superlattice and other mixed structures where the individual inorganic and organic layer thicknesses are varied.<sup>15,16,18,21–30</sup> Further fine-tuning of the properties is possible through various nanostructuring approaches that may turn out to be highly useful in overcoming some of the intrinsic material limitations.

There are only a few preliminary works reported on iron-based ALD/MLD hybrid thin films.<sup>31–33</sup> In two short reports<sup>31,32</sup> the emphasis is on the magnetic properties of the films without details of the deposition process. The precursors employed were FeCl<sub>3</sub> and the aliphatic propargyl alcohol (HC≡C–CH<sub>2</sub>–OH). In the very recent report by Bratvold *et al.*<sup>33</sup> the focus is on the precursor chemistry but the chosen iron precursor Fe(II) β-diketonate-diamine complex, [Fe(hfa)<sub>2</sub>(TMEDA)], (hfa = 1,1,1,5,5,5-hexafluoro-2,4-pentadionate, TMEDA = N,N,N',N'-tetramethylethylenediamine) does not easily allow the deposition of well-controlled superlattice structures as it requires the use of ozone for the oxidation/oxygen source. Then, on the other hand, purely inorganic iron oxide thin films have been deposited by ALD using ferrocene,<sup>9,34–36</sup> iron acetyl acetonate (Fe(acac)<sub>3</sub>),<sup>10</sup> iron tert-butoxide (Fe<sub>2</sub>(OtBu)<sub>6</sub>),<sup>37–39</sup> iron tris(2,2,6,6-tetramethyl-3,5-heptanedionate) (Fe(thd)<sub>3</sub>)<sup>40</sup> and iron chloride (FeCl<sub>3</sub>).<sup>41</sup> From these iron precursors only Fe<sub>2</sub>(OtBu)<sub>6</sub> and FeCl<sub>3</sub> can be oxidized by water; the others require either oxygen or ozone.

Here, in the present work we have systematically investigated various iron precursors together with simple aromatic hydroquinone (HQ) and aminophenol (AP) molecules as the organic precursor; we will introduce a new precursor for the deposition of iron oxides at relatively low temperatures, *i.e.* cyclopentadienyl iron dicarbonyl dimer (Cp<sub>2</sub>Fe<sub>2</sub>(CO)<sub>4</sub>). The linear ALD/MLD type growth is demonstrated with the combination of Cp<sub>2</sub>Fe<sub>2</sub>(CO)<sub>4</sub> and HQ (or AP) and the fact that purely inorganic iron oxide films could be deposited from Cp<sub>2</sub>Fe<sub>2</sub>(CO)<sub>4</sub> using H<sub>2</sub>O as the oxygen source made it also possible to demonstrate the fabrication of iron-oxide based inorganic-organic superlattice structures for the first time.

## Experimental

### Thin-film depositions

The ALD/MLD deposition cycle for iron based inorganic organic hybrid materials consisted of pulses of two precursors, inorganic and organic, and nitrogen (>99.999%; Schmidlin UHPN 3000 N<sub>2</sub> generator) purges in between them. For the iron oxide:organic superlattice structures distilled water was

used as the oxygen source. Four different precursors were initially tested for iron, *i.e.* iron chloride (FeCl<sub>3</sub>, Merck, 95%), iron acetyl acetonate (Fe(acac)<sub>3</sub>; Aldrich, 99.9%), ferrocene (FeCp<sub>2</sub>; Aldrich, 98%) and cyclopentadienyl iron dicarbonyl dimer (Cp<sub>2</sub>Fe<sub>2</sub>(CO)<sub>4</sub>; Strem Chemicals, 99%), while hydroquinone (HQ; Merck, 99.5%) and 4-aminophenol (AP; Aldrich 99%) were employed as the organic precursors.

The depositions were carried out in a commercial flow-type hot-wall ALD reactor (F-120 by ASM Microchemistry Ltd). The solid precursors were set to open precursor boats into the reactor while the water cylinder was held outside the ALD reactor. The pressure was between 2 and 4 mbar and the N<sub>2</sub> flow 300 sccm during the depositions. Silicon (100) substrates (3.5 x 3.5 cm<sup>2</sup>) were used as such. The thin films were deposited at different temperatures in the range of 150–290 °C. The sublimation temperatures were 135, 120, 155 and 45 °C for Cp<sub>2</sub>Fe<sub>2</sub>(CO)<sub>4</sub>, Fe(acac)<sub>3</sub>, FeCl<sub>3</sub> and FeCp<sub>2</sub>, respectively, and 115 and 120 °C for HQ and AP, respectively.

### Characterization

All the sample characterizations for the as-deposited films were carried out within 15 min after taking the samples out from the reactor to get as reliable results as possible. Thickness was measured for each thin-film sample using x-ray reflectivity (XRR; X'Pert MPD PRO Alfa 1, PANalytical). The XRR data were fitted by X'Pert Reflectivity software by PANalytical. Thickness was determined by two different analysis methods, the direct and the Fourier method. Grazing incidence x-ray diffraction (GIXRD; X'Pert MPD PRO Alfa 1, PANalytical; Cu Kα radiation) measurements were performed for films deposited at different temperatures at the incidence angle from 10 to 120°.

Chemical composition of the films was studied with Fourier transform infrared (FTIR; Nicolet magma 750) spectroscopy. Dry air was used for purging the chamber during the measurements. A spectrum of blank Si was subtracted from the spectra to compensate the interference caused by the substrate.

## Results and discussion

**Development of hybrid ALD/MLD process.** From our initial experiments it was revealed that FeCp<sub>2</sub> and Fe(acac)<sub>3</sub> did not react with either HQ or AP molecules in the relevant deposition temperature range. For FeCl<sub>3</sub>, reasonable film growth was realized with both HQ and AP but the films were highly unstable with plenty of chlorine residue. On the other hand, stable and smooth films were obtained when Cp<sub>2</sub>Fe<sub>2</sub>(CO)<sub>4</sub> was employed as the iron precursor. For the further detailed experiments Cp<sub>2</sub>Fe<sub>2</sub>(CO)<sub>4</sub> and HQ precursors were chosen (see Fig. 1).

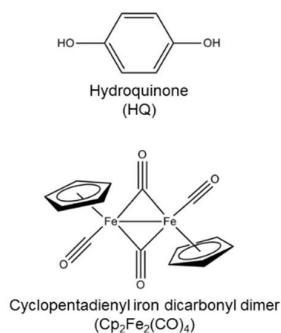


**Fig. 1.** Precursors employed to deposit hybrid iron-based inorganic-organic thin films: hydroquinone (HQ) as the organic precursor and cyclopentadienyl iron dicarbonyl dimer ( $\text{Cp}_2\text{Fe}_2(\text{CO})_4$ ) as the inorganic precursor.

Our first target was to develop a practical ALD/MLD process depositing high-quality thin films of the iron-based inorganic-organic hybrid material, Fe-HQ, where  $\text{Cp}_2\text{Fe}_2(\text{CO})_4$  was employed as the iron precursor. The following pulse/purge lengths were initially selected: 6 s  $\text{Cp}_2\text{Fe}_2(\text{CO})_4$  / 7 s  $\text{N}_2$  / 8 s HQ / 12 s  $\text{N}_2$ . The deposition temperature range was 170–290 °C. In Fig. 2 the film growth rate, *i.e.* growth-per-cycle (GPC), is plotted against the deposition temperature. It is seen that the GPC value rapidly increases with increasing deposition temperature from less than 1 Å/cycle at 170 °C to higher than 10 Å/cycle at 240 °C. The films deposited at the higher temperatures (>200 °C) looked metallic and were too rough for accurate thickness evaluation with XRR such that the thickness of the sample deposited at 250 °C could not be determined anymore. From GIXRD measurements these films were shown to contain metallic iron in crystalline form; see our discussion later on. On the other hand, the films deposited at 170–190 °C looked smooth and homogeneous. As it can be deduced from the increasing GPC values and the crystallization of iron at the higher temperatures (>200 °C), the growth may not meet the requirements of self-limiting growth. Therefore, we decided to investigate the  $\text{Cp}_2\text{Fe}_2(\text{CO})_4$  + HQ process in more detail in the lower temperature range. In Fig. 3 we plot the GPC values for the  $\text{Cp}_2\text{Fe}_2(\text{CO})_4$  + HQ process at 180 °C when the pulse length of one of the two precursors is increased separately. It can be seen that the sufficient pulse lengths to ensure the saturated film growth are 10 s and 15 s for  $\text{Cp}_2\text{Fe}_2(\text{CO})_4$  and HQ, respectively.

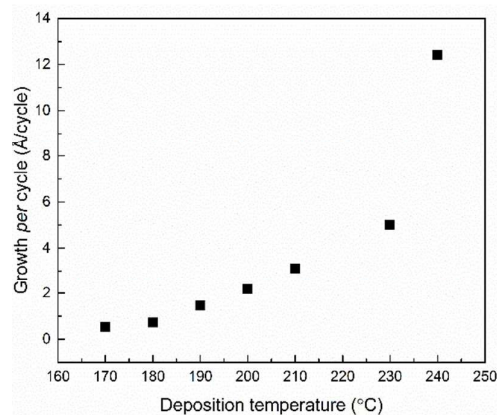


**Fig. 2.** Growth-per-cycle (GPC) for the  $\text{Cp}_2\text{Fe}_2(\text{CO})_4$  + HQ process at different deposition temperatures. The pulse/purge lengths were: 6 s  $\text{Cp}_2\text{Fe}_2(\text{CO})_4$  / 7 s  $\text{N}_2$  / 8 s HQ / 12 s  $\text{N}_2$ .

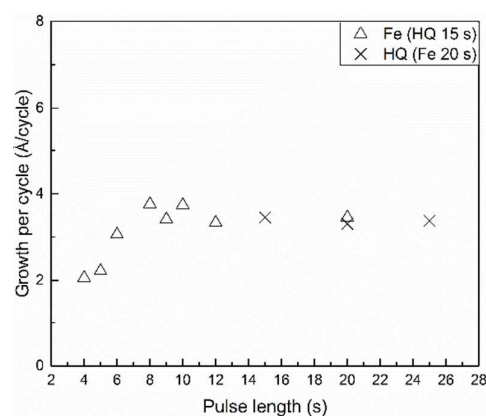


**Fig. 3.** Growth-per-cycle (GPC) for the  $\text{Cp}_2\text{Fe}_2(\text{CO})_4$  + HQ process with different pulse lengths of the two precursors,  $\text{Cp}_2\text{Fe}_2(\text{CO})_4$  ( $\Delta$ ) and HQ (X). The deposition temperature was 180 °C, and the other precursor pulse length was fixed at 20 s and 15 s for  $\text{Cp}_2\text{Fe}_2(\text{CO})_4$  and HQ, respectively, when the other pulse length was varied.

With the precursor pulse/purge lengths of 8–20 s/20–40 s and 15–25 s/30–50 s for  $\text{Cp}_2\text{Fe}_2(\text{CO})_4$  and HQ, respectively, a GPC values were settled between 3.3–3.7 Å/cycle at 180 °C, and even at 150 °C the GPC value was as high as 1.6 Å/cycle. In Fig. 4 we demonstrate that the deposition process behaves in a manner expected for an ideal ALD/MLD process, that is, the film thickness linearly increases with increasing number of deposition cycles.

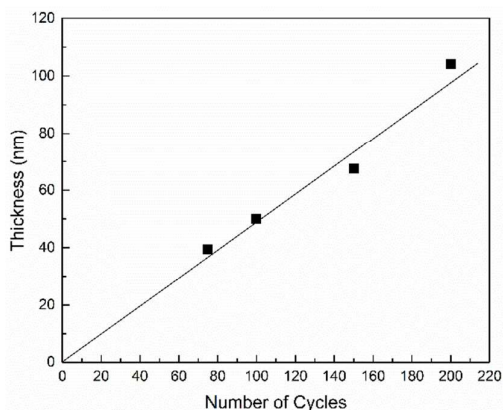


**Fig. 4.** Thickness of the Fe-HQ films versus the number of ALD/MLD cycles at 190 °C, showing an essentially linear dependency. The depositions were carried with the pulse lengths, 10 s  $\text{Cp}_2\text{Fe}_2(\text{CO})_4$  / 20 s  $\text{N}_2$  / 15 s HQ / 30 s  $\text{N}_2$ .

**Properties of hybrid films.** From the GIXRD data shown in Fig. 5 for the Fe-HQ films, the films deposited below 190 °C are completely amorphous; the only diffraction peaks seen are due to the Si substrate. For the films deposited at 200 °C or at the higher temperatures an additional broad peak around  $2\theta \approx 44.9^\circ$  due to metallic iron develops; from the GIXRD pattern recorded with a longer measurement programme for a film deposited at 250 °C (uppermost pattern in Fig. 5) perfect matching to the diffraction pattern of metallic iron could be confirmed. The (partial) crystallinity of the films at the higher deposition temperatures explains the increased surface roughness of these films.

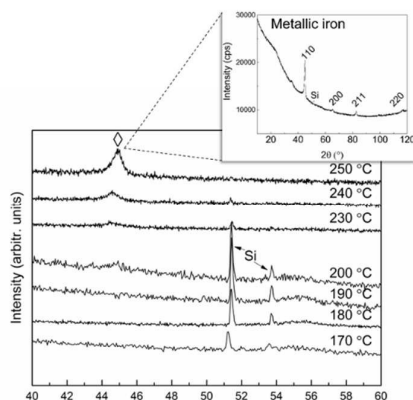


**Fig. 5.** GIXRD patterns for the Fe-HQ-films deposited at different temperatures. Peaks due to metallic iron start to appear at 200 °C. For the film deposited at 250 °C the pattern collected with a longer measurement matches perfectly to that of metallic iron.

FTIR spectra shown in Fig. 6 for the Fe-HQ hybrid films confirm the presence of the organic benzene ring in the films; the peaks caused by C=C stretch are seen at  $1482\text{ cm}^{-1}$  (strong) and  $1595\text{ cm}^{-1}$  (weak), and out of plane bending of C-H bonds at  $801\text{ cm}^{-1}$ . Also, the weak peak of C-O stretch can be seen in the spectra at  $1257\text{ cm}^{-1}$ . Also note that despite the high deposition temperature and crystallization of metallic iron, the signatures of the benzene ring can still be detected in the films

deposited at 290 °C. Also importantly, the data confirm that the reaction occurs already at 170 °C. The variation in peak intensities is mostly due to different thicknesses of the films.

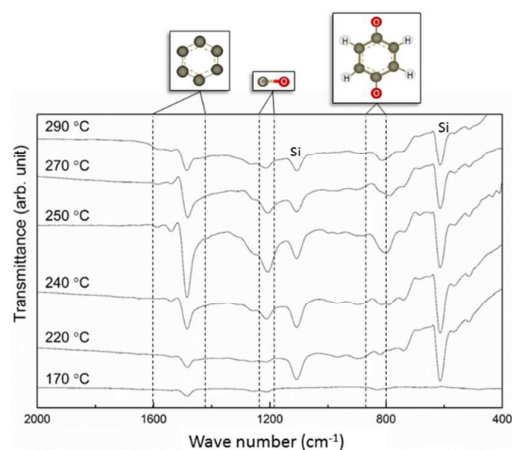


**Fig. 6.** FTIR spectra for the Fe-HQ films deposited at different temperatures. The strongest peaks of aromatic ring and C-O bond can be clearly seen for all the films.

**Stability of hybrid films.** Neither visible changes nor any remarkable changes in FTIR spectra were seen for the hybrid Fe-HQ films when the films were stored in ambient conditions in a covered plastic box. However from the XRR measurement the thickness of the films was found to increase. After one day, depending on the deposition temperature, the thickness of the film was from 2 to 9 % more than right after the deposition, even though the films looked still as good as before. The change in thickness followed the change in deposition temperature, such that the higher the deposition temperature the bigger the change in thickness was. Also the percentage increase in thickness was smaller for a 100-nm film than for a 30-nm film after one day in air. We suggest two possible reasons which could cause the increase in thickness: (i) water molecules from air are intercalated into the inorganic-organic molecular layer structure but only to an extent that was not easily observed by FTIR. As the films deposited at the higher temperatures were more crystalline with more grain boundaries it was easier and faster for the water molecules to penetrate into the film when compared in completely amorphous ones. Another reason could be that (ii) due to increase in temperature, there are more iron species in the structure which can be oxidized. Nevertheless, the amorphous films deposited at low temperature can be stated to be relatively stable in air since the error between measurements is not more than can be affected by the XRR equipment itself.

**Superlattice films.** Superlattice structures were deposited using  $\text{Fe}_2\text{Cp}_2(\text{CO})_4$  as the iron precursor,  $\text{H}_2\text{O}$  as an oxygen source for iron oxide layers and HQ as the organic precursor. The films were deposited at 145 and 160 °C in a different reactor from the one used for the simple hybrid films (with a possibly somewhat different temperature profile/calibration). The total number of cycles was 400 for the films deposited at

145 °C consisting of different oxide:organic ratios of 49:1, 56:1, 66:1, 79:1 and 99:1, corresponding to 4, 5, 6, 7 and 8 iron oxide layers separated with one organic molecular layer. For the depositions at 160 °C the total number of cycles was 500 where the number of oxide layers varied between 4 and 8.

The superlattice period was seen at both deposition temperatures with XRR as small peaks between two bigger ones. The number of the small peaks was two less than the number of oxide layers ( $N-2$ ,  $N$ =number of repetition cycles), as expected.<sup>27</sup> The  $N-2$  trend was clearly seen in superlattice structures having 4-7 oxide layers but not anymore with 8. The XRR patterns are displayed in Fig. 7.

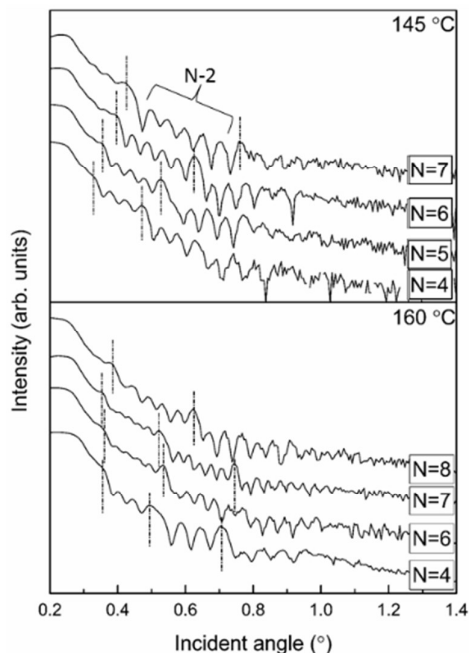


Fig. 7. XRR patterns for the superlattice films deposited at 145 and 160 °C, following the  $N-2$  rule, where the number of smaller peaks between the larger peaks is two less than the number of oxide layers,  $N$ .

The inorganic layers in the superlattice films deposited at 160 °C showed clearly to be of the magnetite ( $\text{Fe}_3\text{O}_4$ ) structure from the GIXRD measurement (Fig. 8). The GPC for pure magnetite films deposited under the same conditions was 2.5 Å/cycle. Diffraction peaks due to the magnetite structure were also clearly detected in the superlattice films deposited at 160 °C. For the films deposited at 145 °C the main diffraction peak of magnetite was still detected but the crystallinity of the films was clearly decreased due to the lower deposition temperature.

It is known that two different materials may hinder the growth of one another. A small decrease in the GPC value could also be seen when adding more and more organic layers into the magnetite films; the GPC decreased from 2.4 Å/cycle to 2.1 Å/cycle when the number of organic layers between the magnetite layers was varied from 3 to 6. We should also mention that we only carried out preliminary experiments to optimize the  $\text{Fe}_2\text{Cp}_2(\text{CO})_4\text{-H}_2\text{O}$  process for  $\text{Fe}_3\text{O}_4$  within the

scope of the present works; details to demonstrate the self-limiting growth will be reported elsewhere.

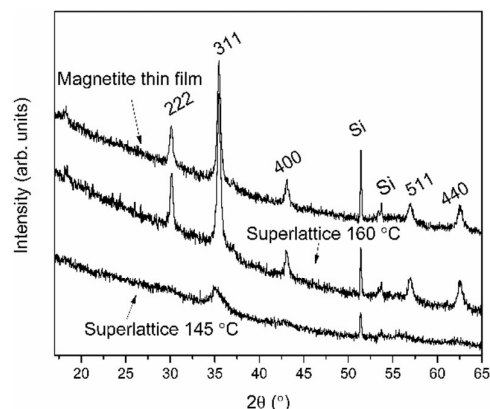


Fig. 8. GIXRD patterns for magnetite and the iron oxide:HQ superlattice films deposited at 145 and 160 °C.

## Conclusions

In this work iron-based hybrid inorganic-organic thin films and oxide:organic superlattice films were successfully deposited by the ALD/MLD technique using cyclopentadienyl iron dicarbonyl dimer as the inorganic precursor. Amorphous Fe-HQ hybrid thin films were obtained in the temperature range of 150-190 °C with an appreciably high GPC value of 3.7 Å/cycle at 180 °C. The film thickness was precisely controlled owing to the ALD-type linear growth. When the deposition temperature exceeded 200 °C metallic Fe started to crystallize.

The oxide:HQ superlattice thin films were fabricated at 145 and 160 °C with different number of HQ layers between thicker iron oxide layers. GIXRD measurements revealed that for the films deposited at 160 °C the iron oxide layers were of the magnetite structure while at 145 °C nearly amorphous films were yielded. The intermittent organic layers did not affect the crystallinity of the films.

Both the simple Fe-HQ hybrid films and the magnetite:HQ superlattice films looked stable by visible observation but XRR measurements revealed that the thickness of the simple Fe-HQ hybrid films increased by 2-9 % when the films were stored for elongated periods. The thicker the film sample was the less the change was implying that the changes mostly occur in the surface layer of the film.

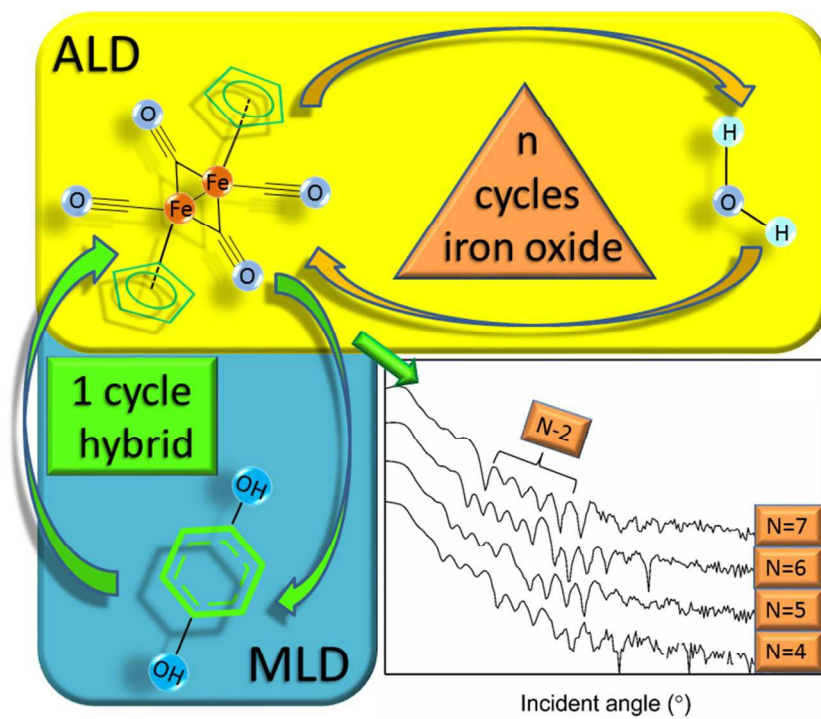
In a wider context we believe that our work is a step ahead in extending the ALD/MLD technique to novel hybrid material compositions based on iron and other interesting 3d transition metals. In particular, we demonstrated the exciting possibility to tailor functional oxide (here magnetite) films by inserting single organic layers between the oxide layers in a well-controlled way.

## Acknowledgement

This work has received funding from the European Research Council under the European Union's Seventh Framework Programme (FP/2007-2013)/ERC Advanced Grant Agreement (No. 339478).

## References

- 1 A. S. Teja and P. Koh, *Prog. Cryst. Growth Charact. Mater.*, 2009, **55**, 22.
- 2 D. A. Wheeler, G. Wang, Y. Ling, Y. Li and J. Z. Zhang, *Energy Environ. Sci.*, 2012, **5**, 6682.
- 3 T. Maruyama and T. Kanagawa, *J. Electrochem Soc.*, 1996, **143**, 1675.
- 4 P. Chauhan, S. Annapoomi and S. K. Tripathi, 1999, **346**, 266.
- 5 T. Hashimoto, T. Yamada and T. Yoko, *J. Appl. Phys.*, 1996, **80**, 3184.
- 6 S. S. Kulkarni and C. D. Lokhande, *Mater. Chem. Phys.*, 2003, **82**, 151.
- 7 S. Capone, M. G. Manera, A. Taurino, P. Siciliano, R. Rella, S. Luby, M. Benkovicova, P. Si and E. Majkova, *Langmuir*, 2014, **30**, 1190.
- 8 N. Serban, C. Ristoscu, G. Socol, N. Stefan, C. N. Mihailescu, M. Socol, S. A. Molenko, Y. N. Petrov, N. T. Gorbachuk and I. N. Mihailescu, *Mater. Res. Bull.*, 2014, **50**, 148.
- 9 B. M. Klahr, A. B. F. Martinson and T. W. Hamann, *Langmuir*, 2011, **27**, 461.
- 10 M. De Ridder, P. C. Van De Ven, R. G. Van Welzenis, H. H. Brongersma, S. Helfensteyn, C. Creemers, P. Van Der Voort, M. Baltes, M. Mathieu and E. F. Vansant, *J. Phys. Chem. B.*, 2002, **106**, 13146.
- 11 M. Leskelä and M. Ritala, *Thin Solid Films*, 2002, **409**, 138.
- 12 S. M. George, *Chem. Rev.*, 2010, **110**, 111.
- 13 H. Zhou and S. F. Bent, *J. Vac. Sci. Technol. A Vacuum, Surfaces, Film.*, 2013, **31**, 040801.
- 14 P. Sundberg and M. Karppinen, *Beilstein J. Nanotechnol.*, 2014, **5**, 1104.
- 15 P. Sundberg, A. Sood, X. Liu and M. Karppinen, *Dalt. Trans.*, 2013, **42**, 15043.
- 16 T. Tynell, I. Terasaki, H. Yamauchi and M. Karppinen, *J. Mater. Chem. A*, 2013, **1**, 13619.
- 17 J.-P. Niemelä and M. Karppinen, *Dalt. Trans.*, 2015, **44**, 591.
- 18 J.-P. Niemelä, A. Giri, P. E. Hopkins and M. Karppinen, *J. Mater. Chem. A*, 2015, **3**, 11527.
- 19 A. A. Dameron, D. Seghete, B. B. Burton, S. D. Davidson, A. S. Cavanagh, J. A. Bertrand and S. M. George, *Chem. Mater.*, 2008, **20**, 3315.
- 20 B. B. Yoon, J. L. O. Patchen, D. Seghete, A. S. Cavanagh and S. M. George, *Chem. Vap. Dep.*, 2009, **15**, 112.
- 21 B. Yoon, B. H. Lee and S. M. George, *J. Phys. Chem. C*, 2012, **116**, 24784.
- 22 A. Sood, P. Sundberg and M. Karppinen, *Dalt. Trans.*, 2013, **42**, 3869.
- 23 A. Sood, P. Sundberg, J. Malm and M. Karppinen, *Appl. Surf. Sci.*, 2011, **257**, 6435.
- 24 B. H. Lee, V. R. Anderson and S. M. George, *ECS Trans.*, 2011, **41**, 131.
- 25 B. H. Lee, V. R. Anderson and S. M. George, *Chem. Vap. Dep.*, 2013, **19**, 204.
- 26 T. Tynell and M. Karppinen, *Thin Solid Films*, 2014, **551**, 23.
- 27 T. Tynell, H. Yamauchi and M. Karppinen, *J. Vac. Sci. Technol. A*, 2014, **32**, 1.
- 28 K. Yoon, K. Han and M. Sung, *Nanoscale Res. Lett.*, 2012, **7**, 1.
- 29 M. Vähä-Nissi, P. Sundberg, E. Kauppi, T. Hirvikorpi, J. Sievänen, A. Sood, M. Karppinen and A. Harlin, *Thin Solid Films*, 2012, **520**, 6780.
- 30 P. Sundberg and M. Karppinen, *Eur. J. Inorg. Chem.*, 2014, 968.
- 31 V. M. Smirnov, E. G. Zemtsova, A. A. Belikov, I. L. Zheldakov, P. E. Morozov, O. G. Polyachonok and V. B. Aleskovskii, *Phys. Chem.*, 2007, **413**, 776.
- 32 V. M. Smirnov, E. G. Zemtsova and P. E. Morozov, *Rev. Adv. Mater. Sci.*, 2009, **21**, 205.
- 33 J. E. Bratvold, G. Carraro, D. Barreca and O. Nilsen, *Appl. Surf. Sci.*, 2015, **347**, 861.
- 34 J. R. Scheffe, A. Francés, D. M. King, X. Liang, B. a. Branch, A. S. Cavanagh, S. M. George and A. W. Weimer, *Thin Solid Films*, 2009, **517**, 1874.
- 35 M. Rooth, A. Johansson, K. Kukli, J. Aarik, M. Boman and A. Hårsta, *Chem. Vap. Depos.*, 2008, **14**, 67.
- 36 A. B. F. Martinson, M. J. DeVries, J. a Libera, S. T. Christensen, J. T. Hupp, M. J. Pellin and J. W. Elam, *J. Phys. Chem. C*, 2011, **115**, 4333.
- 37 J. Bachmann, J. Jing, M. Knez, S. Barth, H. Shen, S. Mathur, U. Gösele and K. Nielsch, *J. Am. Chem. Soc.*, 2007, **129**, 9554.
- 38 B. S. Lim, A. Rahtu and R. G. Gordon, *Nat. Mater.*, 2003, **2**, 749.
- 39 Y. Lin, Y. Xu, M. T. Mayer, Z. I. Simpson, G. McMahon, S. Zhou and D. Wang, *J. Am. Chem. Soc.*, 2012, **134**, 5508–5511.
- 40 M. Lie, H. Fjellvåg and a. Kjekshus, *Thin Solid Films*, 2005, **488**, 74.
- 41 M. Aronniemi, J. Saino and J. Lahtinen, *Thin Solid Films*, 2008, **516**, 6110.



254x190mm (96 x 96 DPI)